

HSM2023-00024

ROBOT ASSISTED STABILIZATION FOR FLEXIBLE WORKPIECES SUBJECTED TO HIGHLY INTERRUPTED CUTTING

R. R. Toth^{1*}, G. Stepan¹

¹Budapest University of Technology and Economics, Department of Applied Mechanics, Budapest, Hungary

*Corresponding author; e-mail: rudolf.toth@mm.bme.hu

Abstract

In many facets of industry, slender workpieces are formed by means of milling processes. These workpieces are especially prone to experience harmful chatter vibrations, which limits quality and productivity. In this paper, a novel solution is proposed where a robotic arm is used to support the workpiece, improving its modal properties and reducing the occurrence of chatter. The paper presents some numerical, analytical and limited experimental results for improving the material removal rate using the robot assisted milling method for low radial immersion processes, such as finishing operations.

Keywords:

chatter, highly interrupted, sampling

1 INTRODUCTION

An essential limiting factor for the efficiency of subtractive manufacturing processes, such as turning or milling, is the appearance of chatter vibrations. These harmful vibrations are the results of regenerative effects, meaning the vibrations during one cut are imprinted on the machined surface which then acts as an excitation in the next cut [Altintas 2012]. There are many approaches to limiting these self-excited oscillations, such as the design of complex tool geometries, increasing the stiffness of the clamped workpiece and machine tool structure or increasing the damping present in the system [Munoa 2016]. Another approach is the direct force control applied to the spindle [Budak 2000]. A new solution to improve the chatter resistance of milling processes of slender workpieces is to support the workpiece opposite to the milling tool using a robotic arm, thus, changing its modal behavior. A similar configuration was studied experimentally in [Ozturk 2018] and [Sun 2019] and was shown to improve productivity. This paper studies the potential and the feasibility of this proposed approach with analytical predictions in simplified models.

Here, low radial immersion processes are investigated, which are described with the model of highly interrupted cutting [Stepan 2005]. The robotic arm is driven using a digital P-controller where the effect of digital sampling is also considered [Stepan 2001]. First, these two basic models are introduced and investigated experimentally. A hardware-in-the-loop system that was developed in [Beri 2020] is used for testing both elementary cases of highly interrupted milling and sampled force control. The combination of these basic models yields the robot assisted

milling method, which is shown to greatly improve the attainable material removal rate, while avoiding chatter.

2 MODEL DESCRIPTION

2.1 Mechanical model

In this section the mechanical model of the robot assisted milling process is discussed. In panel a) of Fig. 1, the sketch of such an arrangement can be seen, while panel b) shows the equivalent single degree of freedom (DoF) model. We assume that the chatter vibrations are related to a single vibration mode of the slender workpiece with parameters m , c and k , since all other structures are significantly stiffer. These modal properties are considered to be uniform along the entire length of the workpiece. The end-effector of the robotic arm is executing a sampled P control algorithm in the x direction in order to attenuate the chatter vibrations, while it follows the milling tool in the y direction with feed v to efficiently counteract the effects of the cutting forces. In the following subsections the two building blocks of this complex model are discussed: the model of highly interrupted cutting and digital force control.

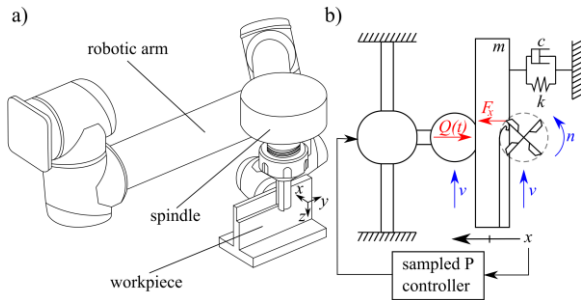


Fig. 1: Sketch of robot assisted milling a). Equivalent mechanical model b).

2.2 Highly interrupted cutting

For low radial immersion milling processes, such as finishing operations, the cutter teeth spend a lot more time in free flight, as opposed to in contact with the material. These short cutting segments are now treated as instantaneous impacts resulting in the model of highly interrupted cutting [Stepan 2005]. The mechanical model of highly interrupted cutting is shown in Fig. 2. The milling tool with $Z = 4$ straight cutting edges has the tooth-pass time $\tau = 60/nZ$, where n is the spindle speed given in rpm. Each tooth-pass is a combination of $(1 - \rho)\tau$ length of free flight and short $\rho\tau$ length impact-like cutting, where parameter ρ describes the level of interruption. Since the cutting is treated as an instantaneous impact, we can define the discrete times $t_j = j\tau$ and simplify the dynamical system into the form (1).

$$x(t_{j+1}) = Ax(t_j) + I_0,$$

$$x(t_j) = \begin{bmatrix} x(t_j) \\ v(t_j) \end{bmatrix}, I_0 = \begin{bmatrix} 0 \\ \frac{\rho\tau}{m} F_0 \end{bmatrix}, \quad (1)$$

where the matrix A has entries

$$A = \begin{bmatrix} A_{11} & A_{12} \\ A_{21} & A_{22} \end{bmatrix},$$

$$A_{11} = \frac{e^{-\zeta\omega_n\tau}}{\sqrt{1-\zeta^2}} \cos(\omega_d\tau - \varepsilon),$$

$$A_{12} = \frac{e^{-\zeta\omega_n\tau}}{\omega_n\sqrt{1-\zeta^2}} \sin(\omega_d\tau),$$

$$A_{21} = \frac{-\omega_n e^{-\zeta\omega_n\tau}}{\sqrt{1-\zeta^2}} \sin(\omega_d\tau)$$

$$+ \frac{\rho\tau}{m} Ka \left[1 - \frac{e^{-\zeta\omega_n\tau}}{\sqrt{1-\zeta^2}} \cos(\omega_d\tau - \varepsilon) \right],$$

$$A_{22} = \frac{e^{-\zeta\omega_n\tau}}{\sqrt{1-\zeta^2}} \left[\cos(\omega_d\tau + \varepsilon) - \frac{\rho\tau}{m\omega_n} Ka \sin(\omega_d\tau) \right]. \quad (2)$$

Note that the natural angular frequency $\omega_n = \sqrt{k/m}$, damping ratio $\zeta = c/2m\omega_n$, damped angular natural frequency $\omega_d = \omega_n\sqrt{1-\zeta^2}$ and the phase parameter is $\varepsilon = \tan^{-1}(\zeta/\sqrt{1-\zeta^2})$. The cutting forces in this model are in the following form during the short cutting

$$F(t) = aK[x(t-\tau) - x(t)] + F_0, \quad (3)$$

where a is the axial depth-of-cut, K is the cutting coefficient depending on the radial immersion and the material properties, while the regenerative term is related to the instantaneous chip thickness being dependent on both the current position of the workpiece and its position at the previous cut. The term F_0 is the force related to steady cutting dependent on the radial and axial depth-of-cut, nominal chip thickness and material properties. This term

does not affect system stability. The stability of dynamical system (1) is determined by the eigenvalues of matrix A , leading to the stability limits of the highly interrupted cutting process presented in [Altintas 2020]. For Hopf-type stability, loss the critical axial depth-of-cut is

$$a_H = \frac{-2m\omega_d \sinh(\zeta\omega_n\tau)}{\rho\tau K \sin(\omega_d\tau)} > a_{Hmin} = \frac{2m\zeta\sqrt{1-\zeta^2}\omega_n^2}{\rho K}, \quad (4)$$

while the process experiences period-doubling induced stability loss at

$$a_{PD} = \frac{m\omega_d \cosh(\zeta\omega_n\tau) + \cos(\omega_d\tau)}{\rho\tau K \sin(\omega_d\tau)} > a_{PDmin} = \frac{m\zeta\sqrt{1-\zeta^2}\omega_n^2}{\rho K}. \quad (5)$$

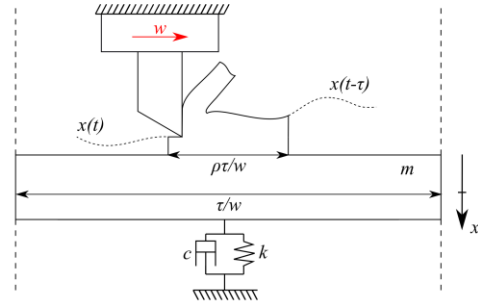


Fig. 2: Mechanical model of highly interrupted cutting.

The stability lobe diagrams generated by formulas (4) and (5) are first shown in Fig. 5.

2.3 Force control with sampling

The second component of the robot assisted milling process is the force control executed by the robotic arm. A simple P control is applied with sampled data of the position of the workpiece, which is used to keep a steady desired force F_d between the workpiece and the end-effector [Whitney 1985]. Since the motion of the workpiece in Fig. 3 is known in a closed form between samples, the dynamical system may be written in the form of equation (6) with discrete times $t_i = ih$:

$$y(t_{i+1}) = By(t_i),$$

$$y(t_i) = \begin{bmatrix} Q(t_i) \\ x(t_i) \\ v(t_i) \end{bmatrix}, \quad (6)$$

where the matrix B has entries

$$B = \begin{bmatrix} 0 & (1-P)k & 0 \\ B_{21} & B_{22} & B_{23} \\ B_{31} & B_{32} & B_{33} \end{bmatrix},$$

$$B_{21} = \frac{1}{k} - \frac{e^{-\zeta\omega_n h}}{k\sqrt{1-\zeta^2}} \cos(\omega_d h - \varepsilon),$$

$$B_{22} = \frac{e^{-\zeta\omega_n h}}{\sqrt{1-\zeta^2}} \cos(\omega_d h - \varepsilon),$$

$$B_{23} = \frac{e^{-\zeta\omega_n h}}{\omega_d} \sin(\omega_d h),$$

$$B_{31} = \frac{\omega_n e^{-\zeta\omega_n h}}{k\sqrt{1-\zeta^2}} \sin(\omega_d h),$$

$$B_{32} = -\frac{\omega_n e^{-\zeta\omega_n h}}{\sqrt{1-\zeta^2}} \sin(\omega_d h),$$

$$B_{33} = \frac{e^{-\zeta\omega_n h}}{\sqrt{1-\zeta^2}} \cos(\omega_d h + \varepsilon). \quad (7)$$

The stability of the controlled motion without cutting forces (6) is dependent on the eigenvalues of matrix \mathbf{B} . The stability diagram in parameters P, h is presented in Fig. 6.

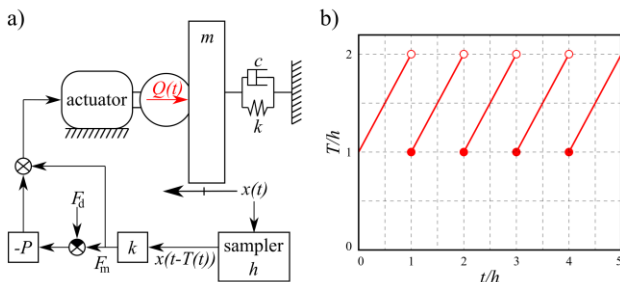


Fig. 3: Mechanical model of 1 DoF sampled force control a). Sawtooth delay caused by sampling time h b).

3 EXPERIMENTAL VALIDATION OF BASIC MODELS

3.1 Overview of the hardware-in-the-loop experimental system

In this section a hardware-in-the-loop (HIL) experimental setup is used to verify the models shown in sections 2.2 and 2.3. The HIL setup is presented in Fig. 4 and consists of a real spindle, laser-based position sensors, a low inductance electromagnetic actuator and a ferrite dummy tool with high saturation suitable for electromagnetic actuation.

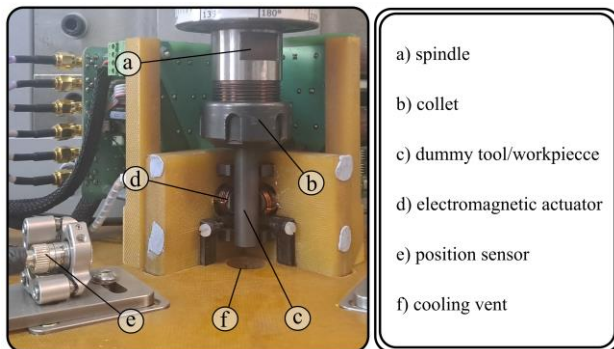


Fig. 4: Hardware-in-the-loop measurement system.

The forces applied by the actuator are updated at 100 kHz frequency using a National Instruments PXIe-8880 real-time computer with two NI7976R FPGA modules. The main purpose of this setup is to test machine tool vibration problems such as turning and milling [Beri 2020]. The fast real time computations allow for generating cutting forces related to any tool geometry and material property. This cost effective and efficient measurement method enables the creation of dense experimental stability charts. The modal properties of the first mode of the dummy tool are approximately $k = 2 \cdot 10^6$ N/m, $c = 4$ Ns/m and $m = 5$ g. These parameters are used throughout the paper.

3.2 Milling measurements in the HIL environment

First let us investigate the validity of the highly interrupted cutting model (1) by comparing it against a measurement made with the HIL system.

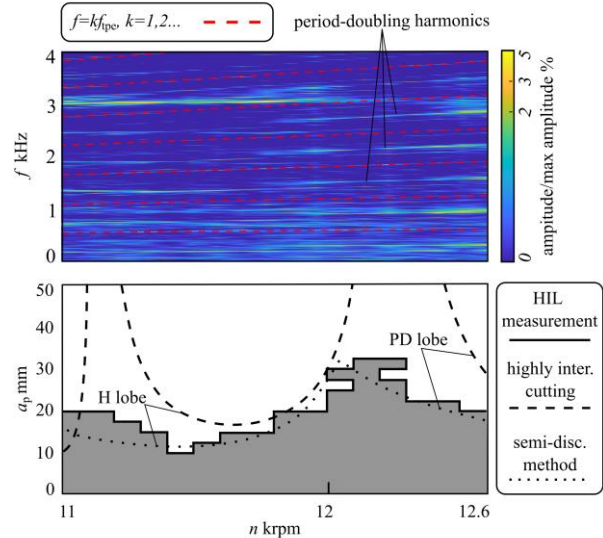


Fig. 5: HIL measurement of milling process and comparison with the highly interrupted cutting model (H meaning Hopf and PD meaning period-doubling bifurcation limit).

The HIL system replicated the actual time dependent cutting coefficients discretized in 256 points. Fig. 5 shows the results of the HIL measurement for milling with $Z = 3$ and radial immersion 1% (leading to $\rho = 0.1$). For more information see [Toth 2023], where this measurement was first presented. In Figure 5, the discrete model of highly interrupted cutting and the measurement shows agreement in stability boundaries and the types of bifurcations match exactly. The stable domain estimated by equations (4) and (5) is larger than the measured one. The differences between this theory and measurement are largely due to the simplification of the cutting as impacts since the numerical prediction made with the semi-discretization method shows improved agreement with the measurements [Insperger 2011].

3.3 Force control in the HIL environment

The built-in versatility of this HIL experimental system allows for the sampled force control problem to be tested as well. We consider the ferrite dummy tool as a dummy workpiece and enact the sampled force control algorithm with sampling frequencies in multiples of 100 kHz. Figure 6 presents the results of the stability measurements compared to the theoretical prediction. The theory and measurements show good agreement. In Fig. 6 several notable control parameter combinations are marked and the related characteristic multipliers are presented. In the following sections, these specific parameter combinations P, h are investigated in the full model of robot assisted milling.

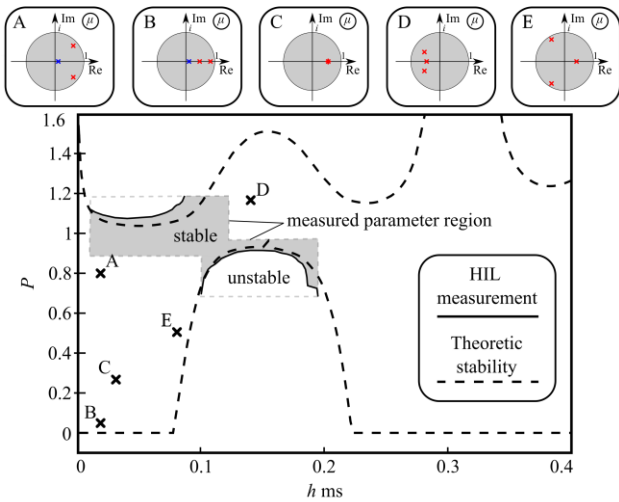


Fig. 6: HIL measurement of sampled force control.

4 ROBOT ASSISTED MILLING

4.1 Numerical approach to the combined discrete problem

In this section, the complete model of robot assisted milling (shown in Fig. 1) is investigated by combining models (1) and (6). The aim of this configuration is to allow for increased productivity by accommodating larger axial depth-of-cuts than what is attainable without the force control present. This also suggests that we should generally investigate parameter combinations where the sampling time is shorter than the tooth-pass period: $h < \tau$. If this condition is not met, the unstable character of the milling process would take effect between samples and deteriorate the finished surface even for a stabilized milling process (note that this condition is not strict and parameters where $\tau/h \cong 1$ might be worth investigating in the future).

The sampling and cutting in models (1) and (6) are both treated as discrete events. This means that the combined model can also be treated discretely, however, since the time steps h and τ can be different, it is not clear what the principal time period of the resulting discrete model is. First, the special case of $\tau/h = r$ with $r \in \mathbb{N}$ is investigated. In this case, the principal time period is simply τ and consists of r subsequent sampling steps and one impact like cutting. This special case leads to the discrete model

$$y(t_{i+1}) = \left(B^r + \frac{\rho\tau}{m} aK(P_1 + P_2 B^r) \right) y(t_i) + J_0, \quad (8)$$

$$P_1 = (-1) \cdot P_2 = \begin{bmatrix} 0 & 0 & 0 \\ 0 & 0 & 0 \\ 0 & 1 & 0 \end{bmatrix}, \quad J_0 = \begin{bmatrix} 0 \\ 0 \\ \frac{\rho\tau}{m} F_0 \end{bmatrix}.$$

The stability of system (8) simplifies to an eigenvalue problem again. Generally, however, the ratio of τ/h is not an integer, so for a dense stability chart in parameters n, a with fixed h , a more general approach is needed. All ratios of τ/h can be arbitrarily accurately approximated with a rational number r/s , where $r, s \in \mathbb{N}$. With this approximation, the combined system has principal time period $rh = s\tau$, which consists of r number of sampling and s number of impact like cutting events. The dynamical system in this general configuration can once more be reduced to an eigenvalue problem, however the matrix in question becomes too complex to provide structured analytical stability boundaries. This rational ratio method is

used as a numerical approach to generate the stability lobe diagrams in section 4.2.

4.2 Continuous approximation of sampled system

For more generic and applicable analytical results, we use a different approach to the rational ratio method of section 4.1. In case of sufficiently large sampling frequency $f_s = 1/h$, the actuation can effectively completely override the oscillations of the workpiece with its damped natural frequency between samples. In this case, it is possible to approximate the discrete sampled force control system (6) using a simple continuous mechanical analog with matching new modal parameters [Budai 2017]. This continuous approximation seems accurate in case of $f_s \geq 4\omega_n/2\pi$, meaning that only about a quarter wave of the natural oscillations can take place between samples. This condition also effectively guarantees that the sampling time $h \leq 2\pi/4\omega_n$ is smaller than the tooth-pass period τ , since the Hopf-type lobe corresponding to the fastest tooth-pass has an asymptote at $\tau = 2\pi/\omega_n$. Figure 7 shows how the sampled and controlled system is substituted for a continuous one, matching the characteristic multipliers of system (6) to the characteristic exponents of the new continuous model.

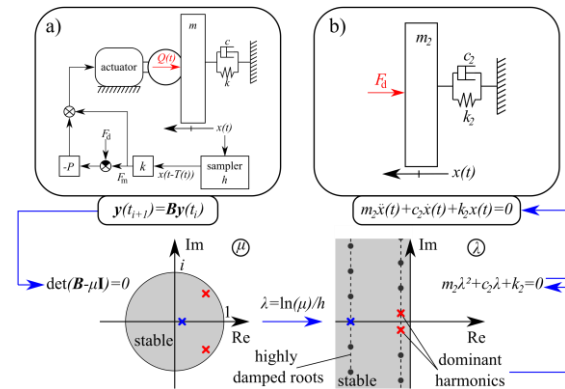


Fig. 7: Substitution of sampled force control system a) for simple oscillator b).

First consider the parameters $h = 2 \cdot 10^{-5}$ s and $P = 0.8$ (point A on Fig. 6) where the dominant characteristic multipliers of the sampled force control system are a pair of complex conjugate roots $\mu_{1,2}$ and the third root is a highly damped real root (like the ones shown in Fig 7.). In this case, the substituting simple oscillator should be underdamped with

$$-\zeta_2 \omega_{n2} \pm i \omega_{d2} = 1/h \cdot \ln(\mu_{1,2}), \quad (9)$$

$$k_2 = Pk, \quad m_2 = \frac{k_2}{\omega_{n2}^2}, \quad c_2 = 2m_2\zeta_2\omega_{n2}.$$

Now the combined force control and highly interrupted cutting system are substituted for a workpiece with modal properties (9) subjected to the same highly interrupted cutting process. This means the stability can be calculated with the same formulas (4) and (5) using the new modal parameters $m_2, \zeta_2, \omega_{n2}$ and ω_{d2} . Figure 8 shows the stability lobe diagrams resulting from the previously discussed model with cutting conditions $Z = 4$, $\rho = 0.08$ and $K = 2.5 \cdot 10^8$ N/m².

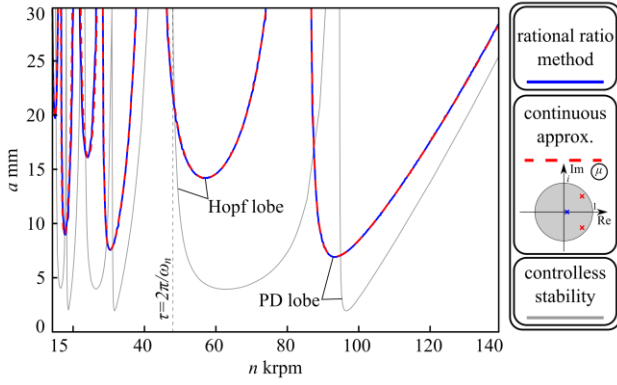


Fig. 8: Stability lobe diagram for the robot assisted milling, in case of underdamped control behavior.

In Fig. 8, the continuous approximation shows good agreement with the rational ratio method in section 4.1. The force control results in significantly improved stability compared to no control at all, which is expected since we could essentially tune the problematic modal properties of the slender workpiece to be more beneficial.

The example in Fig. 8 could already greatly improve the stability of the milling process, however, there are even more possibilities there. We can tune the control parameters, such that the characteristic multipliers of the force control system alone are all stable real valued ($h = 2 \cdot 10^{-5}$ s and $P = 0.04$, point B on Fig. 6). Ignoring the highest damped real root, we can now consider substituting the force-controlled workpiece with an overdamped one with parameters:

$$\lambda_{1,2} = 1/h \cdot \ln(\mu_{1,2}),$$

$$k_2 = Pk, \quad m_2 = \frac{k_2}{\lambda_1 \lambda_2}, \quad c_2 = 2m_2 \zeta_2 \omega_{n2}. \quad (10)$$

The overdamped workpiece exhibits significantly different behavior from the previous ones and being exposed to highly interrupted cutting, it presents the system in form

$$\mathbf{x}(t_{j+1}) = \mathbf{A}_2 \mathbf{x}(t_j) + \mathbf{I}_0, \quad (11)$$

where the matrix \mathbf{A}_2 has entries

$$\mathbf{A}_2 = \begin{bmatrix} U_{11} & U_{12} \\ U_{21} & U_{22} \end{bmatrix}, \quad U_{11} = \frac{\lambda_2 e^{\lambda_1 \tau} - \lambda_1 e^{\lambda_2 \tau}}{\lambda_2 - \lambda_1}, \quad U_{12} = \frac{e^{\lambda_2 \tau} - e^{\lambda_1 \tau}}{\lambda_2 - \lambda_1},$$

$$U_{21} = \frac{\lambda_1 \lambda_2 e^{\lambda_1 \tau} - \lambda_1 \lambda_2 e^{\lambda_2 \tau}}{\lambda_2 - \lambda_1} + \frac{\rho \tau}{m} Ka \left[1 - \frac{\lambda_2 e^{\lambda_1 \tau} - \lambda_1 e^{\lambda_2 \tau}}{\lambda_2 - \lambda_1} \right],$$

$$U_{22} = \frac{\lambda_2 e^{\lambda_2 \tau} - \lambda_1 e^{\lambda_1 \tau}}{\lambda_2 - \lambda_1} - \frac{\rho \tau}{m} Ka \frac{e^{\lambda_2 \tau} - e^{\lambda_1 \tau}}{\lambda_2 - \lambda_1}. \quad (12)$$

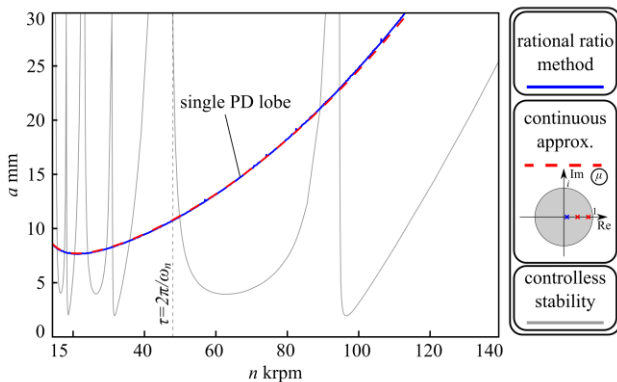


Fig. 9: Stability lobe diagram for the robot assisted milling, in case of overdamped control behavior.

The overdamped system is actually resistant to Hopf-type stability loss and the single stability boundary related to the period-doubling bifurcation is

$$a_{2PD} = \frac{m_2(\lambda_2 - \lambda_1)(e^{\lambda_1 \tau} + 1)(e^{\lambda_2 \tau} + 1)}{2\rho \tau K e^{\lambda_2 \tau} - e^{\lambda_1 \tau}} > a_{2PDmin} = \frac{m_2 \lambda_2 \lambda_1}{\rho K}. \quad (13)$$

Figure 9 shows the stability lobe diagrams resulting from this overdamped case. The rational ratio method and continuous approximation agree closely once more. The overdamped nature of the substituted workpiece erases the stability lobes, and a single period-doubling limit remains. This can greatly improve stability, particularly for high spindle speeds (in the region of the first original lobes).

Another interesting case to investigate is when the force-controlled system on its own presents the fastest possible settling in hopes of achieving even more improvements in stability. This occurs when all characteristic multipliers are equal to each other at $h = 3.23 \cdot 10^{-5}$ s and $P = 0.2684$ (point C on Fig. 6). In this case, not one of the real roots may be discarded, so a different, third order substitution with no classical mechanical analogy can be made leading to an equation of motion excluding the cutting forces:

$$j_2 \ddot{x}(t) + m_2 \dot{x}(t) + c_2 x(t) + k_2 x(t) = 0, \quad (14)$$

where the parameters are

$$\lambda = \lambda_{1,2,3} = 1/h \cdot \ln(\mu),$$

$$k_2 = Pk,$$

$$c_2 = -Pk \frac{\lambda_1 \lambda_2 + \lambda_1 \lambda_3 + \lambda_2 \lambda_3}{\lambda_1 \lambda_2 \lambda_3},$$

$$m_2 = Pk \frac{\lambda_1 + \lambda_2 + \lambda_3}{\lambda_1 \lambda_2 \lambda_3},$$

$$j_2 = \frac{-Pk}{\lambda_1 \lambda_2 \lambda_3}. \quad (15)$$

Considering workpiece with properties (14) and (15) subjected to the cutting conditions leads to a three-dimensional discrete model that is lengthy, but solvable resulting in the single period-doubling lobe seen in Fig. 10. Once more, the two methods show good agreement and the increase in stability is significant. In fact, even lower and more attainable spindle speed regions (15 – 40 krpm) become highly stable, which is a very promising result for the effectiveness of this chatter attenuation technique.

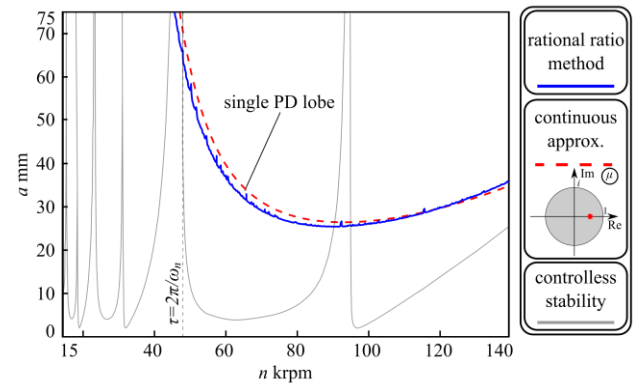


Fig. 10: Stability lobe diagram for the robot assisted milling, in case of fastest settling control behavior.

4.3 Additional complex cases

In section 4.2, we were able to show numerical and analytical predictions for the stability of robot assisted milling for a wide spectrum of parameters. However, there are some special parameter combinations of the force-

control system that present even more strange dynamics and related stability lobe diagrams, which are yet to be accurately estimated using the continuous approximation. The first case includes a real characteristic multiplier of the force-controlled system in the left-half plane (see point D in Fig. 6), which results in strange characteristic exponents that may need even higher order dynamical systems to approximate accurately. The control parameters corresponding to point E in Fig. 6 presents a more conventional stability lobe diagram with both Hopf and period-doubling lobes, but with a different arrangement compared to the one in Fig. 8. Figure 11 shows the stability charts calculated with the rational ratio method for the two complex cases. While even these cases shown in Fig. 11 can increase stability compared to the system without any control, they are less desirable than the cases in section 4.2.

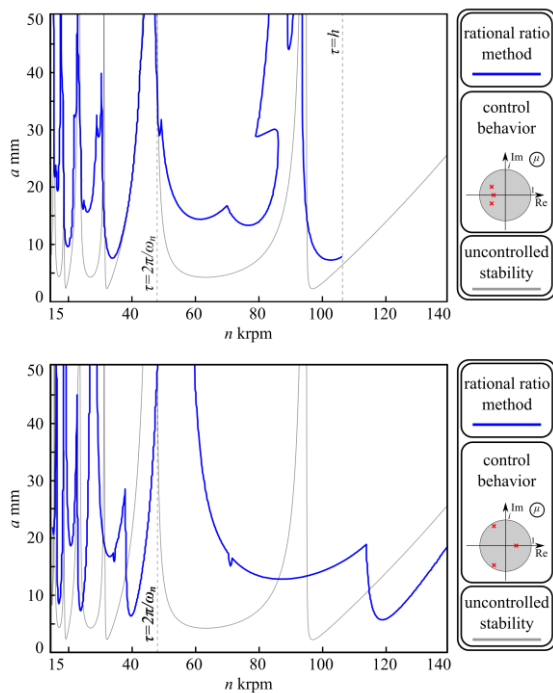


Fig. 11: Stability lobe diagram for the robot assisted milling, in complex cases (point D on top and point E on the bottom).

5 SUMMARY

The chatter suppression technique of using a robotic arm to support a slender workpiece was proposed and investigated. First, the model of highly interrupted cutting and sampled force control was introduced to describe the milling process and the effect of the robotic arm on the workpiece. These models were also experimentally investigated and validated by constructing dense stability charts using our hardware-in-the-loop system.

The combination of these two models describes the robot assisted milling. In the combined model, the paper presents two methods for stability prediction. First, the ratio of tooth-pass to sampling was approximated with a rational number allowing for a discrete dynamical model to be constructed and analyzed. This technique is applicable numerically. The second proposed method, applicable to sufficiently fast sampling, is based on the substitution of the sampled control system with an alternative workpiece matching in modal behavior. This method resulted in

analytic formulas for the stability curves. The two methods show good agreement.

The combined model of robot assisted milling displayed greatly improved chatter resistance, particularly in the case, where the sampled controller was tuned to the fastest settling. Here, a large highly stable domain was observed even for relatively small spindle speeds.

There are, however, some parameter combinations that have not yet been fully explored, including smaller sampling time applications. The current methods propose minimum sampling frequency $f_s \geq 4\omega_n/2\pi$, enforcing a necessity of potentially high computation power. Another avenue to improve the predictive power of the discussed models is to consider a more accurate description of the milling process than the highly interrupted cutting one, since even the experimental methods revealed some inaccuracy of this model compared to numerical solutions provided by the semi-discretization. The experimental validation of the combined robot assisted milling model is also needed in the future.

6 ACKNOWLEDGEMENTS

The research reported in this paper has been supported by the Hungarian National Research, Development and Innovation Office (NKFI-KKP-133846, NKFI-K-132477).

7 REFERENCES

- [Altintas 2012] Altintas Y. Manufacturing Automation: Metal Cutting Mechanics, Machine Tool Vibrations, and CNC Design (2nd ed.). Cambridge University Press, Cambridge (2012)
- [Altintas 2020] Altintas Y., Schmitz, T., and Kilic, Z. M. Chatter Stability of Machining Operations. ASME. J. Manuf. Sci. Eng. November 2020; 142(11): 110801.
- [Beri 2020] Beri B., Miklos A., Takacs D. and Stepan G. Nonlinearities of hardware-in-the-loop environment affecting turning process emulation. Int. J. Mach. Tools Manuf., 2020, 157: Article 103611
- [Budai 2017] Budai Cs., Kovacs L. L., Kovacs J., Stepan G. Effect of dry friction on vibrations of sampled-data mechatronic systems. Nonlinear Dynamics, 2017, 88, 349-361
- [Budak 2000] Budak E. and Kops L., Improving Productivity and Part Quality in Milling of Titanium Based Impellers by Chatter Suppression and Force Control. CIRP Annals, 2000, 49(1), Pages 31-36
- [Insperger 2011] Insperger T. and Stepan G. Semi-Discretization for Time-Delay Systems – Stability and Engineering Applications. Springer New York, 2011
- [Munoa 2016] Munoa, J., Beudaert, X., Dombovari, Z., Altintas, Y., Budak, E., Brecher, C. and Stepan, G. Chatter suppression techniques in metal cutting. CIRP Annals, 2016, 65(2), 785-808
- [Ozturk 2018] Ozturk E., Barrios A., Sun C., Rajabi S. and Munoa J. Robotic assisted milling for increased productivity. CIRP Annals, 2018, 67(1), 427-430
- [Stepan 2001] Stepan G. Vibrations of machines subjected to digital force control. Int. Journal of Solids and Structures, March 2001, 38(10-13), 2149-2159
- [Stepan 2005] Stepan G., Insperger T., Szalai R. Delay, parametric excitation, and the nonlinear dynamics of cutting processes. International Journal of Bifurcation and Chaos, 2005, 15(9), 2783- 2798

[Sun 2019] Sun C., Kengne L.F.P., Barrios A., Mata S. and Ozturk E. Form Error Prediction in Robotic Assisted Milling. *Procedia CIRP*, 2019, 82, 491-496

[Toth 2023] Toth R.R. and Stepan G. Bifurcation scenarios in the hardware-in-the-loop experiments of highly interrupted milling processes. *Nonlinear Dynamics*, 2023, 1573-269X

[Whitney 1985] Whitney, D.E., Historical perspective and state of the art in robot force control. *International Journal of Robotics Research*, 1985, 6, 3-14.